Sensors and Materials, Vol. 34, No. 12 (2022) 4651–4668
MYU Tokyo

S & M 3135

Application of Real-time Positioning Systems to a Forest Stand for Precision Forest Management

Hyun-Min Cho,[1†] Jae-Heun Oh,[2] Jin-Woo Park,[1†]
Yun-Sung Choi,[2] Jung-Soo Lee,[1] and Sang-Kyun Han[1*]

[1]Division of Forest Sciences, College of Forest and Environmental Sciences, Kangwon National University, 1, Kangwondaehak-gil, Chuncheon-si, Gangwon-do 24341, South Korea
[2]Forest Technology and Management Research Center, National Institute of Forest Science, 498, Gwangneungsumogwon-ro, Soheul-eup, Pocheon-si, Gyeonggi-do 11186, South Korea

(Received October 31, 2022; accepted December 19, 2022)

Keywords: precision forestry, real-time positioning system, global navigation satellite system, inertial navigation system, positioning accuracy

There is an increasing demand for modern information and communications technologies (ICTs), such as light detection and ranging (LiDAR), photometric stereo, and mechanized forestry machines, for achieving more precise and efficient forest management. Simultaneously, the real-time positioning (RP) system has gained prominence as an essential peer technology. However, the conventional RP system, a single-band global navigation satellite system (GNSS), is inadequate for utilization with newly proposed precision forestry management systems. Therefore, we assessed the applicability of two alternative RP systems, GNSS real-time kinematic (GNSS-RTK) and embedded GNSS and inertial navigation system (INS), which can be applied to actual forest operations. We also analyzed the relationship between positioning error and various environmental factors. Consequently, the embedded GNSS/INS (EGI) showed better performance, with a root mean squared error (RMSE) of 1.42 m, than the GNSS-RTK (1.52 m), and its RMSE significantly decreased after sensor heading calibration (p <0.05) by 15 min of warm-up driving. In addition, both GNSS-RTK and EGI demonstrated a negative correlation between the RMSE and forest canopy coverage ($p < 0.05$). In this study, we identified the existing limitations and opportunities of proposed RP systems applied within the forestry industry, allowing for the development of a more suitable RP system for precision forestry management in future research.

1. Introduction

More than 70% of the forest area in South Korea is rapidly approaching harvesting age (over 50 years old); therefore, a substantial increase in timber harvesting is expected in the near future.(1) However, the number of workers and operators in the forestry industry is gradually declining, resulting in higher operating costs that hinder the continued effectiveness of managing

*Corresponding author: e-mail: hsk@kangwon.ac.kr
†These authors contributed equally to this work.
https://doi.org/10.18494/SAM4214

ISSN 0914-4935
https://myukk.org/

and harvesting the forest resources.[2,3] As a result, a concerted effort has lately been made to adopt cutting-edge technologies, such as light detection and ranging (LiDAR),[4] information and communications technologies (ICTs),[5] photometric stereo,[7] autonomous driving (AD), and mechanized operation systems, in forestry activities to facilitate precision forest management.[7]

Specifically, 3D forest inventory construction technology using LiDAR simultaneous localization and mapping (LiDAR SLAM) has advanced rapidly in recent years. LiDAR SLAM is a high-precision, less labor-intensive method for forest inventory surveying that can provide basic information on each tree in a forest, such as the diameter at breast height (DBH), tree height, size of the crown, and tree density.[8] These types of data can be used to aid in the selection of trees optimal for removal in the thinning operation, allowing for more efficient forest management that promotes maximum timber growth and enhances the capacity of the forest to absorb carbon. In addition, LiDAR SLAM can be used to obtain the absolute coordinates of each tree.[9,10] However, to effectively utilize the acquired data in actual thinning operations, the operator must be able to precisely navigate the coordinates of target thinning trees. Therefore, a high-precision real-time positioning (RP) solution is essential for operators; without it, identifying certain thinning trees in a dense forest would be exceedingly difficult.[11]

The most commonly used RP system in the forestry industry is a single-band standalone global navigation satellite system (GNSS) receiver. This system tends to be imprecise, with a positioning error of approximately 5–10 m, especially under low-visibility conditions such as in urban areas and forest stands.[12,13] Nonetheless, as the demand for a more accurate RP system in the forestry industry increases, several solutions are being presented, including GNSS real-time kinematic (GNSS-RTK) and embedded GNSS & inertial navigation system (GNSS/INS) receivers.[14,15]

The GNSS-RTK employs multiband satellite signals, which can greatly reduce the multipath effect caused by the possible signal interference by the ionosphere, mountainous environment, and buildings in urban areas, resulting in improved positioning accuracy.[16] Furthermore, the GNSS-RTK achieves cm-order precision by utilizing an independent base station that can simultaneously transmit correction data to the rover receiver using a radio frequency (RF) signal. However, there are still some limitations to using GNSS-RTK in the forestry industry because of the fact that the rover uses the RF signal for both correction data and satellite signal reception, resulting in frequent RF signal loss in areas where the space between the base station and the rover is obscured. When the signal of correction data transmitted from the base station is lost, the rover is forced to reacquire it, and the positioning error rapidly increases during this time.[17]

The embedded GNSS/INS (EGI) is a commonly used positioning sensor in the automotive and defense industries. It comprises integrated GNSS and INS and employs the Kalman-filter algorithm to continuously calculate position using INS sensor data at locations where GNSS is unavailable.[18] An INS sensor consists of gyros and accelerometers for measuring the angular rate of the three-dimensional axis and velocity, respectively. However, similarly to other positioning solutions, the EGI system is susceptible to drift errors, a type of positioning error. Drift errors are cumulative errors that occur when the EGI is in an unaided state, and only INS sensors are used for position calculation. The drift errors gradually increase with time but can be

corrected by calibrating the heading of the vehicle using GNSS whenever the signal becomes available again.[19]

To achieve precision forest management in the future, rigorous adaptation of the RP system is required. Therefore, the purpose of this study was to assess the adaptability of each RP system (GNSS-RTK and EGI) to actual forest operations. The specific objectives of this study were to (1) compare the positioning errors of the two RP systems in the forest, (2) analyze the relationship between the positioning error and forest environmental factors, and (3) elucidate the potential limitations of each RP system.

2. Materials and Methods

2.1 Overall experimental design

The main goal of this study was to compare the applicability of GNSS-RTK and EGI in a forest. The experiment was designed with two parts: accuracy comparison and relationship analysis (Fig. 1). In the accuracy comparison, the positioning error and its variance were compared. In addition, for the relationship analysis, a total of three forest environmental factors were used: area type, warm-up driving, and canopy coverage. The area type was divided into three categories: forested, conjunction, and open. Conjunction refers to the portion of the road connecting the forested area and the open area. Warm-up driving in this study is defined as the duration of driving before the experiment and set to 0, 15, and 30 min to determine the changes in positioning accuracy during this time.

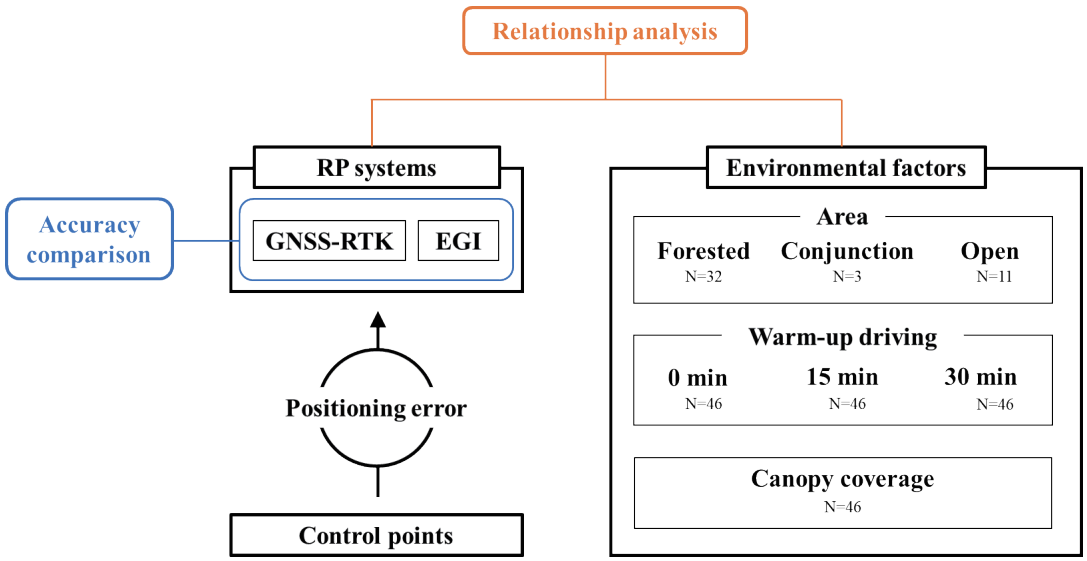

Fig. 1. (Color online) Experimental design of the study.

2.2 Study site

The experiment was conducted on August 26 and 27, 2021, on the road of the Forest Technology and Management Research Center, National Institute of Forest Science, South Korea (Fig. 2). The total length of the road was 456 m, and it was divided into three types of area: forested, conjunction, and open (Table 1). The forested area had a dynamic longitudinal gradient (average: 6.4°), and its canopy coverage was high (average: 85.6%) (Fig. 3). In contrast, the open area was level (average longitudinal gradient: 1.7°) and contained a few trees along the roadway (average canopy coverage: 17.8%). In addition, the average DBH and height of trees in the forest were 40 cm and 22 m, respectively.

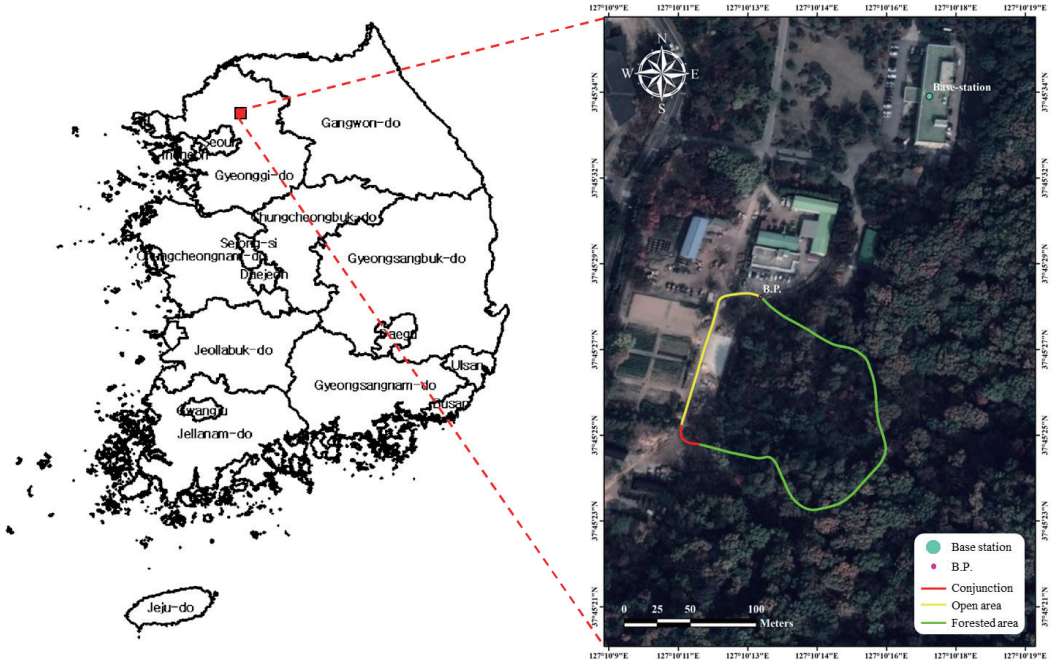

Fig. 2. (Color online) Location of the study site.

Table 1
General characteristics of study area.

Items	Area type			Total
	Forested	Conjunction	Open	
Distance (m)	310.8	20.6	124.6	456.0
Longitudinal gradients (°)	6.4	2.0	1.7	—
Canopy coverage (%)	85.6	7.0	17.8	64.8
Forest type	Broadleaf forest			
Species	*Konara Oak*			
Age class	IX			
DBH[a] (cm)	40			
Height (m)	22			

[a]diameter at breast height

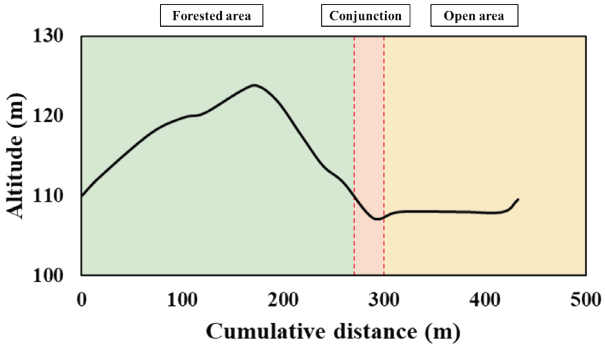

Fig. 3. (Color online) Topographical characteristic of study area by area type.

2.3 Accuracy of RP systems

2.3.1 Control data collection

To evaluate the positioning accuracy of RP systems, it is necessary to first acquire the control data in order to calculate the positioning error. In this study, control data refer to the coordinates of each representative location on the experimental track of road; a total of 46 control points at 10 m intervals were collected (Fig. 4). The control data were collected using a GNSS receiver, R2 (Trimble, United States) (Table 2). All control point coordinates were collected by the static survey method based on the networked transport of radio technical commission for maritime services via Internet protocol data from the reference station, also known as the virtual reference station surveying method. The survey was conducted for 15 epochs at each point with a horizontal root mean squared accuracy (HRMS) of less than 0.01 m and a vertical root mean squared accuracy (VRMS) of less than 0.015 m.

2.3.2 RP system data collection

For the two RP systems proposed in this study (GNSS-RTK and EGI), the equipment listed in Table 3 were utilized. Propak-V3 (Novatel, Canada) and DL-V3 (Novatel, Canada) were adopted as a rover and base station, respectively, for the GNSS-RTK, whereas EGIS-N400D (Korea) was used for the EGI system.

The base-station antenna of the GNSS-RTK was positioned on the rooftop of a building approximately 200–300 m away from the experimental site. The antennas of the GNSS-RTK rover and EGI were mounted on the rooftop rack of a vehicle, and the GNSS-RTK and EGI loggers were placed inside the trunk and rooftop carrier, respectively (Fig. 5). The GNSS antennas of GNSS-RTK and EGI were positioned at the same vertical height and at the center of the width of the vehicle to ensure that each sensor could follow the same path during the driving experiment. The experimental data, which consisted of the coordinates of the points logged along the track by 1 s, were collected during 12 trips to the study site at speeds of 6–8 km/h. Among the 12 driving trials, each of the three warm-up driving trials consisted of four

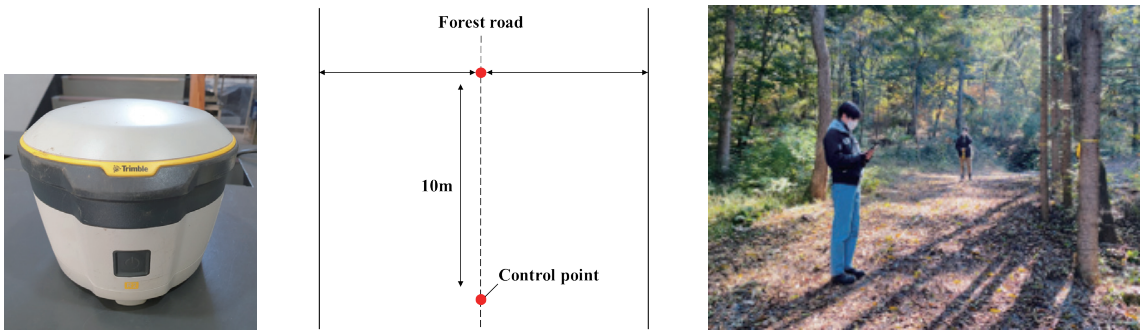

(a) (b) (c)

Fig. 4. (Color online) (a) GNSS receiver utilized for the collection of control data. (b) Method of control points measurement. (c) Photo of measuring control points using GNSS receiver.

Table 2
Technical specifications of equipment used for logging control data.

Items	Specification
Type of sensor	GNSS receiver
Name of model	R2
Signal tracking	GPS L1/L2 GLONASS L1/L2 Galileo L1/L2 BeiDou L1/L2 QZSS L1/L2
Positioning output rate	1/2/5 Hz
Positioning precision	Differential GPS HRMS 0.25 m + 1 ppm VRMS 0.50 m + 1 ppm Static HRMS 3 mm + 0.5 ppm VRMS 5 mm + 0.5 ppm RTK HRMS 10 mm + 1 ppm VRMS 20 mm + 1 ppm Network RTK HRMS 10 mm + 0.5 ppm VRMS 20 mm + 0.5 ppm
Hardware	Size: 14 (diameter) × 11.4 (height) cm^2 Weight: 1.08 kg

replications. The first trial started with no warm-up driving, whereas the second and third trials started after 15 and 30 min of warm-up driving, respectively.

2.3.3 Analysis of positioning error in RP systems

To quantify the positioning error of the two positioning systems, the positioning error was defined as the horizontal distance between the X and Y coordinates measured by each positioning system and the control point coordinates. The distance was calculated using a haversine formula

Table 3
(Color online) Technical specifications of equipment used for each RP system.

Specification	GNSS-RTK		EGI
	Rover	Base station	
Type of sensor	GNSS receiver	GNSS receiver	GNSS/INS
Name of model	Propak-V3	DL-V3	EGIS-N400D
Signal tracking	GPS L1/L2/L5 GLONASS L1/L2 SBAS L1/L2 L-band 1	GPS L1/L2/L5 GLONASS L1/L2 SBAS L1/L2 L-band 1	GPS L1/L2 GLONASS L1/L2 Galileo E1/E5 BeiDou B1/B2
Positioning output rate	<50 Hz	<50 Hz	<100 Hz
Positioning (Pose) precision	HRMS 1 cm + 1 ppm	HRMS 1 cm + 1 ppm	HRMS ± 3m VRMS ± 3m Roll ± 0.2° Pitch ± 0.2° Yaw ± 0.3°
Hardware	Size: 185 × 160 × 71 mm^3 Weight: 1.0 kg	Size: 185 × 162 × 76 mm^3 Weight: 1.3 kg	Size: 61 × 45 × 90 mm^3 Weight: <350 g
Photo			

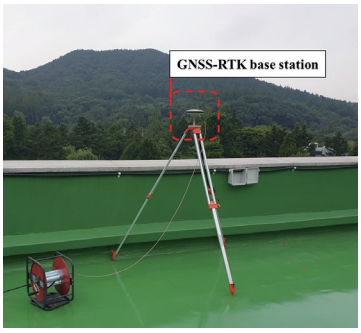

(a)

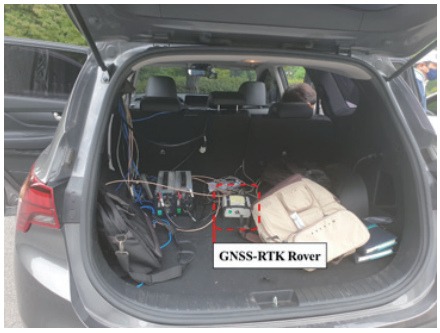

(b)

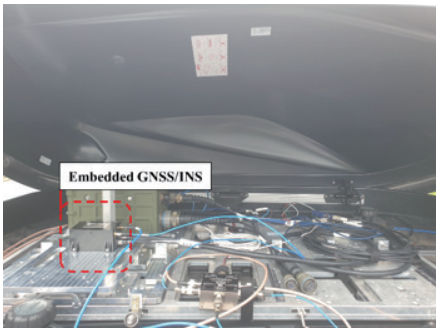

(c)

(d)

Fig. 5. (Color online) (a) Rooftop of the building where the GNSS-RTK base station was installed. (b) Trunk of the sport utility vehicle (SUV) where the GNSS-RTK rover was installed. (c) Rooftop cargo carrier of SUV vehicle where the EGI sensor was mounted. (d) SUV vehicle used for the experimental driving.

[Eq. (1)] under the assumption that the Earth is a spheroid, and the coordinate system adopted for both the control and experimental data logging was WGS84. The Earth's radius was defined as 6371 km for distance calculation using the haversine formula. Since driving replications in this study (a total of 12) were numeric, the root mean squared error (RMSE) was calculated to determine the representative positioning error at each control point [Eq. (2)].

$$Positioning\ error\left(d\right) = 2r \times \arcsin\sqrt{sin^2\left(\frac{\varphi_2 - \varphi_1}{2}\right) + \cos(\varphi_1)\cos(\varphi_2)sin^2\left(\frac{\lambda_2 - \lambda_1}{2}\right)} \quad (1)$$

Here, φ_1 and φ_2 are the latitudes of points 1 and 2, respectively; λ_1 and λ_2 are the longitudes of points 1 and 2, respectively; and r is the radius of the sphere.

$$RMSE = \sqrt{\frac{\sum_{i=1}^{n}\left(d_i\right)^2}{n}} \quad (2)$$

n is the number of driving replications and d_i is the ith observed positioning error.

2.4 Analysis of relationships with environmental factors

2.4.1 Canopy coverage data collection

The canopy coverage was surveyed using a spherical densitometer to analyze the relationship between canopy coverage and positioning accuracy in the forest. The canopy coverage was surveyed at a total of 17 points spaced at 25-m intervals on average and four times by aspect (N, S, W, E) at each point (Table 4).

The canopy coverage in the forested area was 88%, whereas the conjunction and open areas only had canopy coverages of 10 and 14% on average, respectively. The canopy coverage at each control point was derived by using an interpolated linear canopy coverage graph (Fig. 6).

2.4.2 Analysis of variance (ANOVA) between the RMSE and the area type and warm-up driving time

To determine the effect of the two treatments, namely, area type and warm-up operation, on positioning accuracy, a one-way ANOVA test was conducted on the average RMSE for each treatment category. First, the Levene equal-variance test was performed, then the sum of the square between (SSB), the sum of the square error (SSE), and the sum of the square total (SST) were calculated to assess the variance of RMSE across treatments and within each treatment using Eq. (3), Eq. (4), and Eq. (5), respectively. The differences were greater with larger variance values. The significance of the difference between the groups was verified at a 95% significance level.

Table 4
Measured canopy coverage along the driving track.

Point No.	Area type	Distance (m)	Cumulative distance (m)	Aspect				Canopy coverage (%)
				East	West	North	South	
B.P.	Forested	—	0.0	68.8	63.6	67.8	60.5	65.2
1	Forested	21.9	21.9	80.2	77.1	79.2	75.0	77.9
2	Forested	18.7	40.6	91.7	89.6	88.6	90.6	90.1
3	Forested	24.5	65.1	92.7	91.7	89.6	88.6	90.6
4	Forested	30.3	95.4	93.8	87.5	86.5	89.6	89.3
5	Forested	24.3	119.7	94.8	85.4	91.7	89.6	90.4
6	Forested	29.8	149.5	93.8	91.7	92.7	89.6	91.9
7	Forested	18.7	168.2	94.8	91.7	92.7	93.8	93.2
8	Forested	18.1	186.3	87.5	86.5	82.3	87.5	86.0
9	Forested	23.9	210.2	94.8	93.8	90.6	95.8	93.8
10	Forested	37.8	248.0	97.9	95.8	91.7	96.9	95.6
11	Forested	22.3	270.3	94.8	92.7	95.8	93.8	94.3
12	Conjunction	22.0	292.3	11.6	8.5	7.4	10.6	9.5
13	Open	26.3	318.6	27.2	19.9	16.8	11.6	18.9
14	Open	29.6	348.2	7.4	10.6	8.5	8.5	8.7
15	Open	26.0	374.2	12.6	16.8	37.6	18.9	21.5
16	Open	32.4	406.6	6.4	9.5	4.3	5.4	6.4

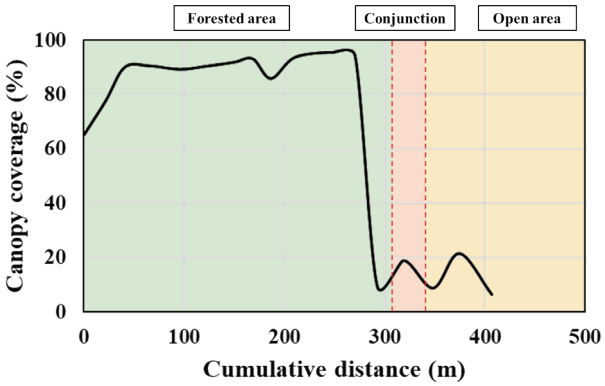

Fig. 6. (Color online) Canopy coverage along the driving track in the study site.

$$SSB = n\sum_{i=1}^{m}\left(\bar{X}_i - \bar{X}\right)^2 \tag{3}$$

$$SSE = \sum_{i=1}^{m}\sum_{k=1}^{n}\left(X_{ik} - \bar{X}_i\right)^2 \tag{4}$$

$$SST = SSB + SSE = \sum_{i=1}^{m}\sum_{k=1}^{n}\left(X_{ik} - \bar{X}\right)^2 \tag{5}$$

Here, n is the number of observations per cell, m is the number of groups, i is the group treatment level, k is the cell member, $\overline{X}_i$ is the group mean, $\overline{X}$ is the grand mean, and X_{ik} is the individual observation.

2.4.3 Correlation analysis between RMSE and canopy coverage

To determine the association between the RMSE and canopy coverage, the Pearson correlation coefficient (r) was used in the correlation analysis because the data of both groups were not ordinal [Eq. (6)]. Pearson's correlation coefficient ranged from −1 to 1, with a greater positive strength between variables when the number was closer to 1 and the opposite when it was closer to −1.

$$r = \frac{n\left(\sum XY\right) - \left(\sum X\right)\left(\sum Y\right)}{\sqrt{\left[n\sum X^2 - \left(\sum X\right)^2\right]\left[n\sum Y^2 - \left(\sum Y\right)^2\right]}} \tag{6}$$

Here, n is the number of paired stocks, ΣXY is the sum of products of the paired stocks, ΣX is the sum of the X scores, ΣY is the sum of the Y scores, ΣX^2 is the sum of the squared X scores, and ΣY^2 is the sum of the squared Y scores.

3. Result and Discussion

3.1 Accuracy of RP systems

3.1.1 Control data

A map of the control point locations is presented in Fig. 7. Control points were dispersed as follows: 32 points in forested areas, three points in conjunction areas, and 11 points in open areas (Table 5).

3.1.2 Accuracy of RP systems

As the driving trajectory was logged using the two RP systems depicted in Fig. 8, the GNSS-RTK measurements were more frequently interrupted than that of the EGI system. The observed disruption on GNSS-RTK was attributed to the loss of the radio signal from the base station owing to high canopy coverage and position dilution of precision (PDOP) in forested areas. However, in open areas, the GNSS-RTK trajectory was more accurate than that of the EGI because of the high strength of the radio signal from the base station as there are no existing obstacles (Fig. 9). According to the driving trajectory of EGI, the cumulative shift error, which is the most common type of positioning error when employing an INS sensor,[20] was noted, which may have been caused by wheel slip during driving. Even though the average of the total RMSE was higher with EGI (1.35 m) than with GNSS-RTK (1.31 m), GNSS-RTK showed an

Fig. 7. (Color online) Location of control points along the experimental driving track.

Table 5
Status of control points in the study site

Items	Area type			Total
	Forested	Conjunction	Open	
Number of points	32	3	11	46

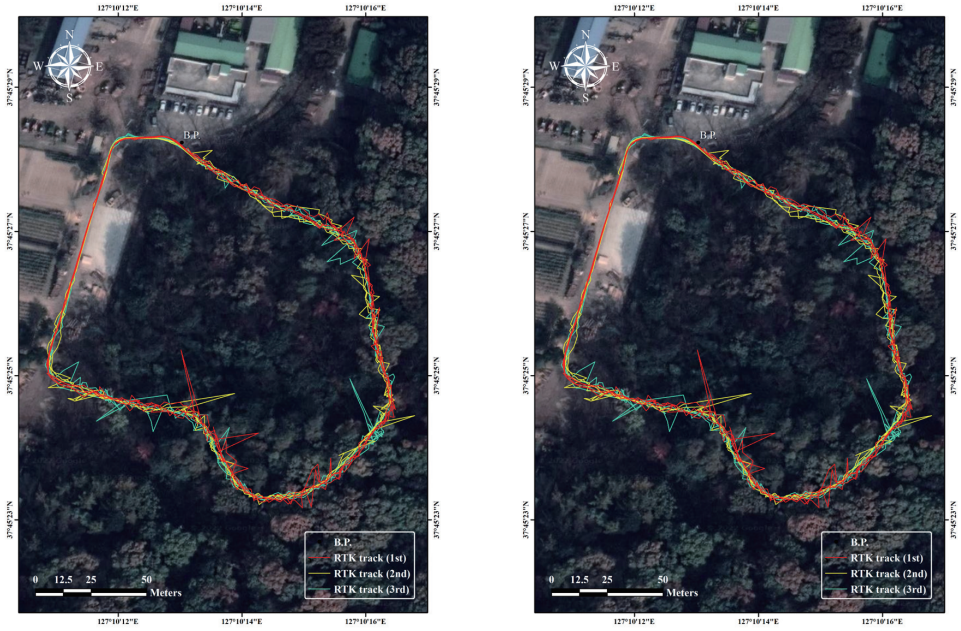

(a) (b)

Fig. 8. (Color online) Track maps of the positions logged with (a) GNSS-RTK and (b) EGI systems.

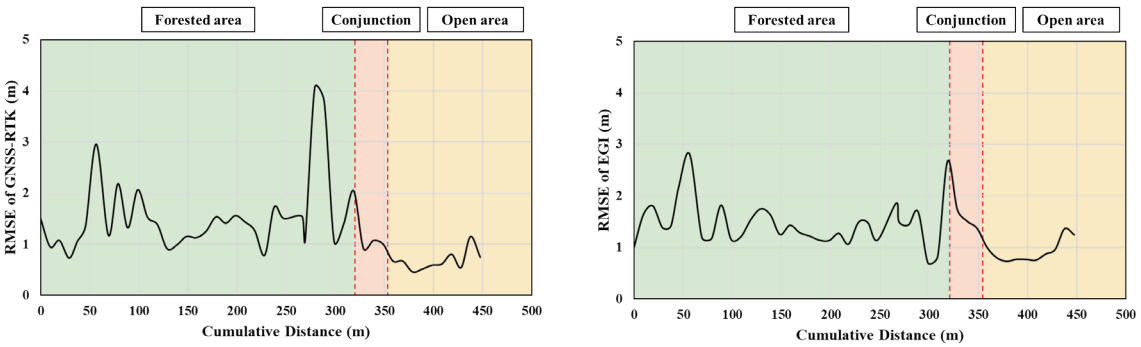

(a) (b)

Fig. 9. (Color online) Variation in RMSE with increasing cumulative distance for (a) GNSS-RTK and (b) EGI system.

Table 6
General statistics on the total RMSE of RP systems.

RMSE (Unit: m)	*N*	GNSS-RTK				EGI			
		Avg.	Min.	Max.	SD[a]	Avg.	Min.	Max.	SD[a]
Total	46	1.31	0.45	4.06	0.74	1.35	0.69	2.80	0.46

[a]standard deviation.

approximately 36% higher RMSE standard deviation (SD) (Table 6). Both RP systems showed excellent accuracy in comparison to the positioning error RMSE of the mobile GNSS-RTK device that Feng *et al.*[21] tested in a broadleaf forest.

3.2 Relationship between positioning accuracy and environmental factors

3.2.1 Area types

As determined by a statistical analysis of RMSE by area type, both GNSS-RTK and EGI showed the lowest RMSE in forested areas, with averages of 0.70 and 0.96 m, respectively (Table 7). As predicted by the trajectory, the RMSE of EGI was lower than that of GNSS-RTK in forested areas, whereas it was higher in open areas. However, EGI had the highest RMSE in conjunction areas (1.97 m), where the slope gradients were steeper than in both forested and open area, causing more frequent vibrations that could affect the accuracy of the internal gyro sensor. Kaartinen *et al.*[22] determined the positioning accuracy of the GNSS+ inertial measurement unit (IMU) to be 0.6–0.8 m RMSE, achieving a suitable accuracy standard (1 m) for utilization in further forestry operations.

Prior to the ANOVA test, an equal-variance test was conducted, and both GNSS-RTK and EGI showed an equal variance of the average RMSE between the area types ($p > 0.05$, Table 8). Consequently, using Duncan's post-hoc analysis, significant variations in average RMSE were found between forested and open areas in GNSS-RTK, whereas significant variations were observed across all area types in EGI ($p < 0.05$, Fig. 10). An evident increase in RMSE of EGI in the conjunction area was observed and presumed to originate from the bumps experienced during driving owing to the dynamic slope change and poor road condition.

Table 7
General statistics of RMSE for each driving area type.

RMSE (Unit: m)	*N*	GNSS-RTK				EGI			
		Avg.	Min.	Max.	SD[a]	Avg.	Min.	Max.	SD[a]
Forested	32	1.52	0.73	4.06	0.77	1.42	0.69	2.80	0.41
Conjunction	3	1.34	0.91	2.04	0.61	1.97	1.50	2.67	0.62
Open	11	0.70	0.45	1.15	0.21	0.96	0.72	1.36	0.25

[a]standard deviation.

Table 8
Result of one-way ANOVA for response variable RMSE by driving area type.

RP system	*N*	Equal-variance test		ANOVA test				
		Levene	*P*-value	SSB[a]	SSE[b]	SST[c]	*F*	*P*-value
GNSS-RTK	46	1.670	0.200	5.542	19.394	24.936	6.144	0.004[d]
EGI	46	1.464	0.243	2.955	6.494	9.449	9.783	0.000[d]

[a]sum of squares between groups.
[b]sum of squares error within groups.
[c]sum of squares total.
[d]$p < 0.05$.

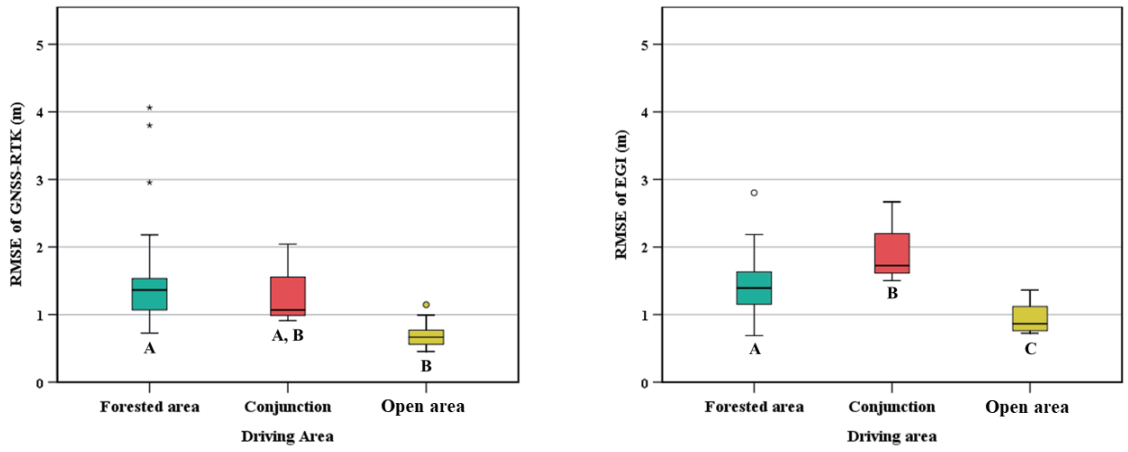

(a) (b)

Fig. 10. (Color online) Mean RMSE of (a) GNSS-RTK and (b) EGI by driving area type.

3.2.2 Warm-up driving time

To evaluate the impact of warm-up driving on positioning accuracy as part of the calibration process for the sensors in each positioning system, the change in the RMSE values of GNSS-RTK and EGI were analyzed based on warm-up driving time (0, 15, and 30 min). In GNSS-RTK, a small increase in average RMSE was observed as warm-up driving time increased (Table 9). In contrast, the longer the warm-up driving time, up to 15 min, the higher the accuracy of EGI, as evidenced by an approximately 21% decrease in RMSE. However, EGI showed an increase of RMSE again after 30 min of warm-up driving, possibly as a consequence of the over-calibration of the inertial heading sensor in EGI as a result of the longer calibration period than the threshold time for adequate sensor calibration.

On the basis of the equal-variance test, a one-way ANOVA was conducted using Duncan's and Dunnett's post-hoc analyses for GNSS-RTK and EGI, respectively (Table 10). ANOVA using average RMSE as the response variable showed that warm-up driving time has a significant effect for EGI ($p < 0.05$), whereas no significant difference was found for GNSS-RTK ($p > 0.05$). Furthermore, EGI demonstrated a significant reduction in positioning error after 15 min of warm-up driving compared with the first driving trial without warm-up driving, followed by a modest increase at 30 min of warm-up driving (Fig. 11). Also, Li *et al.*[23] found that rotating IMU regularly for approximately 15–50 min can significantly reduce the drift and shift of each accelerometer and gyroscope.

Table 9
General statistics of RMSE by warm-up driving time.

RMSE (Unit: m)	*N*	GNSS-RTK				EGI			
		Avg.	Min.	Max.	SD[a]	Avg.	Min.	Max.	SD[a]
0 min	46	1.03	0.36	2.49	0.51	1.43	0.47	2.96	0.63
15 min	46	1.38	0.42	4.27	0.74	1.06	0.50	2.93	0.51
30 min	46	1.29	0.40	6.25	1.21	1.31	0.67	2.86	0.60

[a]standard deviation

Table 10
Result of one-way ANOVA for response variable RMSE by warm-up driving time.

RP system	*N*	Equal-variance test		ANOVA test				
		Levene	*P*-value	SSB[a]	SSE[b]	SST[c]	*F*	*P*-value
GNSS-RTK	46	2.654	0.074	0.616	34.868	35.484	1.192	0.307
EGI	46	7.383	0.001[d]	4.897	39.532	44.429	8.237	0.000[d]

[a]sum of squares between groups.
[b]sum of squares error within groups.
[c]sum of squares total.
[d]$p < 0.05$

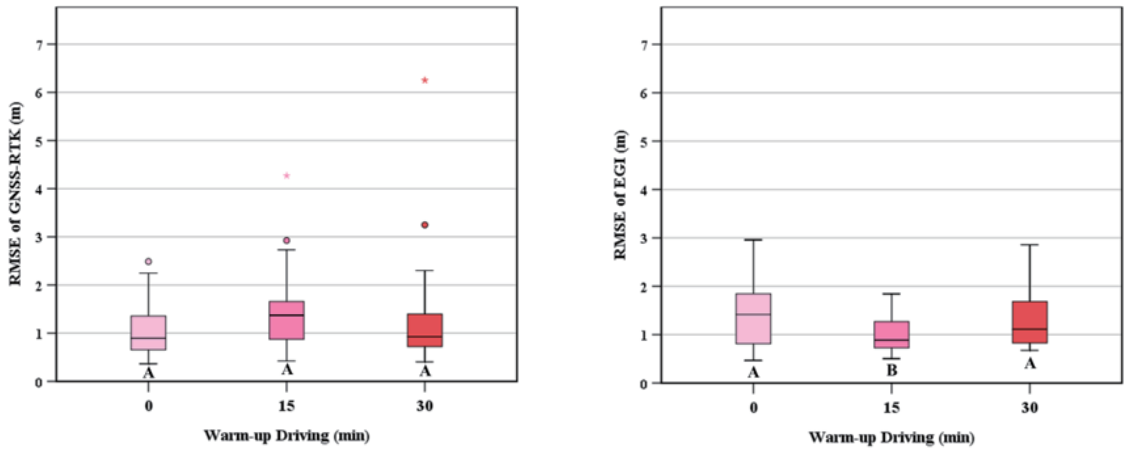

(a) (b)

Fig. 11. (Color online) Mean RMSE of (a) GNSS-RTK and (b) EGI versus warm-up driving time.

3.2.2 Canopy coverage

As GNSS-RTK and EGI systems use satellite-received location data for coordinate positioning utilizing inertial GNSS sensors, their positioning accuracy is consequently affected by sky visibility, particularly in relation to tree canopy coverage in a forest. The result of the correlation analysis between the RMSE and canopy coverage of both positioning systems yielded significant results ($p < 0.05$) with positive Pearson's coefficients of 0.441 and 0.513 (Table 11), respectively. Nonetheless, the cumulative positioning error of EGI showed a lower RMSE variance than that of GNSS-RTK in areas with high canopy coverage of greater than 80% (Fig. 12). Another study revealed that to obtain a positioning accuracy greater than 2.5 m, GNSS should be combined with a RTK or precise-point positioning system in forests with canopies that cover more than 70% of the sky.[24]

As a general assessment of the experiment in this study, we would like to highlight a few limitations of the experimental design in order to guide and enhance future studies.

(1) In this study, each trial consisted of four driving replications, and the driving tracks of a total of 12 replications were not at the exact same horizontal location. Despite the driver making every attempt to drive along the designated track, a small amount of error that cannot be accounted for is inevitable. A specific function that enables a vehicle to drive automatically along the directed waypoints in order to maintain an even driving path might help alleviate this problem.

Table 11
Result of correlation analysis between RMSE and canopy coverage.

RMSE–Canopy coverage	*N*	Pearson's	*P*-value
GNSS-RTK	46	0.441	0.002[a]
EGI	46	0.513	0.000[a]

[a]$p < 0.05$.

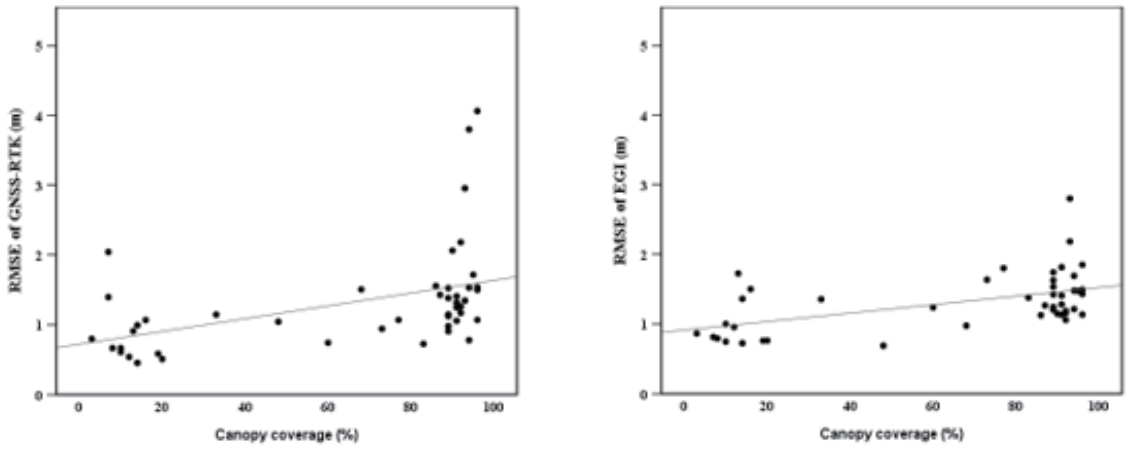

(a) (b)

Fig. 12. RMSE distribution plotted against canopy coverage for (a) GNSS-RTK and (b) EGI.

(2) Regarding the referencing process between the coordinates of control points and the matching coordinates logged with each sensor, it was desirable for the sensors to pass the exact control points throughout the driving experiment in order to determine the precise error of logged data. Nonetheless, all driving replications in this study relied on the experience of the driver to pass the marked control points along the track.

Despite the aforementioned limitations, the possible error of the calculated RMSE is unlikely to have a significant influence on the presented results, because the targeted acceptable accuracy for the intended purpose of the sensors was approximately 1 m, whereas the distance error caused by the experimental design, which was estimated on the basis of the driver's experience, was less than 20 cm.

4. Conclusion

In this study, we analyzed the overall positioning accuracy of two RP systems in the forestry industry, GNSS-RTK and EGI, to provide the basic analytic data necessary for employing a suitable positioning system for mechanized thinning operations. Three factors were analyzed relative to positioning accuracy: area type, warm-up driving time, and forest canopy coverage.

It was demonstrated that EGI performed more accurately than GNSS-RTK in the forested area. However, since EGI is an integrated sensor comprising GNSS and INS, it is known that the performance of the integrated GNSS sensor affects the accuracy of the final output. For example, if the internal GNSS sensor collects coordinate data with insufficient accuracy, it will inevitably result in the accumulation of sensor bias error, particularly in forested areas where GNSS signal loss is common. Nevertheless, recently developed GNSS sensors, which are known to have a rapid reacquisition time, can enable EGI to obtain more precise coordinate data during brief periods of sky-visibility improvement.

In addition, we discovered that the warm-up driving period had a substantial impact on the positioning accuracy of EGI. As the EGI sensor system consists of automotive-grade inertial sensors, such as gyros and accelerometers, variable bias and sensor drifts are commonplace. However, through this study, it was found that these biases could be reduced by calibrating the sensor with the adoption of a warm-up driving period which could provide a heading bias correction rate. Moreover, another noteworthy finding of the study was that exceeding the significance threshold of warm-up driving time (15 min) might reset the bias correction of inertial sensors, resulting in an increase in the positioning error of EGI. This could be adjusted by the careful selection of the internal algorithm settings of the sensor; thus, the user should be mindful not to over-calibrate the sensor prior to usage.

The canopy coverage was shown to have a positive correlation with the positioning error of both GNSS-RTK and EGI, corroborating the findings of previous research. In terms of applicability, while both GNSS-RTK and EGI showed satisfactory positioning errors of approximately 1 m, the variance of GNSS-RTK revealed positioning errors of up to approximately 4 m, which represents insufficient reliability for matching certain trees with the coordinates of their location. However, given that the base-station model (DL-V3) utilized in the GNSS-RTK system was a dated model, there is the possibility of enhancing the performance of

the GNSS-RTK system by incorporating newer models of equipment, such as sensors and radio modems with higher transmit power.

During the study, a limitation that may have to be considered for adapting the proposed positioning systems to actual forest operations was discovered. Concern existed regarding the installation location of the sensor on the forestry operating machine. In the scenario of the operation procedure using the sensor-equipped machine, it is important for the operator to identify the exact tree at a certain coordinate in order to avoid felling erroneous trees; hence, the sensor should necessarily be in close proximity to the trees. For this purpose, it might be best to install the sensor on the dangle-head or arm of the machine. However, this poses considerable hazards, such as potential damage during operation, as well as the degradation of localization due to vibrations and impacts. Thus, it is preferable to mount the sensor on a portion of the machine cabin, whereby the method of distance calibration from the cabin to the machine arm can be used to provide real-time localization.

Acknowledgments

This research was carried out with the support of the "R & D Program for Forest Science Technology (Project No. 2021359D10-2223-BD01)" provided by the Korea Forest Service (Korea Forestry Promotion Institute).

References

1 Statistical Yearbook of Forestry (Korea Forest Service, Republic of Korea, 2020) p. 448 (in Korean).
2 K. D. Kim, B. H. Jung, and C. S. Kim: J. KIFR **14** (2010) 33. https://doi.org/10.34272/forest.2010.14.4.004
3 B. H. Jung, C. S. Kim, and K. D. Kim: J. KIFR **14** (2010) 26. https://doi.org/10.34272/forest.2010.14.4.003
4 Y. Sun, X. Jin, T. Pukkala, and F. Li: Remote Sens. **14** (2022) 1125. https://doi.org/10.3390/rs14051125
5 M. H. Ahmad, M. E. William, L. N. Juma, and M. S. Dawood: Int. J. Nat. Resour. Ecol. Manage. **7** (2022) 1. https://doi.org/10.11648/j.ijnrem.20220701.14
6 Q. Gao and J. Kan: Remote Sens. **15** (2022) 9. https://doi.org/10.3390/rs14092064
7 L. G. Bont, M. Fraefel, F. Frutig, S. Holm, C. Ginzler, and C. Fischer: J. Environ. Manage. **302** (2022) 114099. https://doi.org/10.1016/j.jenvman.2021.114099
8 S. Cha, H. W. Jo, M. Kim, C. Song, H. Lee, E. Park, J. Lim, D. Schepaschenko, A. Shvidenko, and W. K. Lee: J. Appl. Remote Sens. **16** (2022) 2. https://doi.org/10.1117/1.JRS.16.024503
9 M. Tulldahl, J. Rydell, J. Holmgren, J. Nordlof, and E. Willen: Proc. SPIE 11160, Electro-Optical Remote Sensing XIII (SPIE, 2019) 1116005. https://doi.org/10.1117/12.2533299
10 Q. Li, P. Nevalainen, J. P. Queralta, J. Heikkonen, and T. Westerlund: Remote Sens. **12** (2020) 11. https://doi.org/10.3390/rs12111870
11 G. Eloise, Zimbelman, and R. G. Keefe: PLoS ONE **13** (2018) 1. https://doi.org/10.1371/journal.pone.0191017
12 Y. C. Lee: KSCE J. Civil Environ. Eng. Res. **28** (2008) 4D.
13 K. Y. Lee and G. Kim: Korean J. Nat. Conserv. **8** (2014) 2. https://doi.org/10.11624/KJNC.2014.8.2.186
14 M. N. Cahyadi and I. Rwabudandi: Proc. E3S Web Conf. **94** (2019) 03015. https://doi.org/10.1051/e3sconf/20199403015
15 H. Zhang, J. Zheng, G. Dorr, H. Zhou, and Y. Ge: Arab. J. Sci. Eng. **39** (2014) 237. https://doi.org/10.1007/s13369-013-0861-1
16 L. Lau, H. Tateshita, and K. Sato: J. Navig. **68** (2015) 5. https://doi.org/10.1017/S0373463315000168
17 J. Jackson: Real-time Kinematic Positioning: Background, Assessment and Forecasting (ProQuest, Minnesota, 2018) p. 93.
18 A. Angrisano: GNSS/INS Integration Methods (University of Messina, Messina, 2010) p. 168.
19 J. Lee and H. Kim: J. Inst. Electron. Eng. Korea **49** (2012) 11.

20 H. K. Lee, J. Wang, C. Rizos, B. Li, and W. Y. Park: Proc. 6th Int. Symp. Satellite Navigation Technology Including Mobile Positioning & Location Services (SatNav, 2003) 43.
21 T. Feng, S. Chen, Z. Feng, C. Shen, and Y. Tian: Remote Sens. **13** (2021) 2325. https://doi.org/10.3390/rs13122325
22 H. Kaartinen, J. Hyyppa, M. Vastaranta, A. Kukko, A. Jaakkola, X. Yu, J. Pyorala, X. Liang, J. Liu, Y. Wang, R. Kaijaluoto, T. Melkas, M. Holopainen, and H. Hyyppa: Forests **2015** (2015) 6. https://doi.org/10.3390/f6093218
23 K. Li, P. Gao, L. Wang, and Q. Zhang: Math. Problems Eng. **2015** (2015) 768174. https://doi.org/10.1155/2015/768174
24 J. Huang, Y. Guo, X. Li, N. Zhang, J. Jiang, and G. Wang: Forests **13** (2022) 1591. https://doi.org/10.3390/f13101591